Chiral unitary approach to *S*-wave meson baryon scattering in the strangeness $S=0$ sector

T. Inoue,* E. Oset, and M. J. Vicente Vacas
Departamento de Física Teórica and IFIC, Centro Mixto Universidad de Valencia-CSIC, Institutos de Investigación de Paterna, Apartado Correos 22085, E-46071 Valencia, Spain

(Received 31 October 2001; published 14 February 2002)

We study the *S*-wave interaction of mesons with baryons in the strangeness $S=0$ sector in a coupled channel unitary approach. The basic dynamics is drawn from the lowest order meson-baryon chiral Lagrangians. Small modifications inspired by models with explicit vector meson exchange in the *t* channel are also considered. In addition the $\pi\pi N$ channel is included and shown to have an important repercussion in the results, particularly in the isospin 3/2 sector. The $N^*(1535)$ resonance is dynamically generated and appears as a pole in the second Riemann sheet with its mass, width, and branching ratios in fair agreement with experiment. A $\Delta(1620)$ resonance also appears as a pole at the right position although with a very large width, coming essentially from the coupling to the $\pi\pi N$ channel, in qualitative agreement with experiment.

DOI: 10.1103/PhysRevC.65.035204 PACS number(s): 12.39.Fe, 12.40.Yx, 13.75.−n

I. INTRODUCTION

The introduction of effective chiral Lagrangians to account for the basic symmetries of QCD and its application through χPT to the study of meson-meson interaction [1] or meson-baryon interaction [2–5] has shed new light on these problems and allowed a systematic approach. Yet, χPT is constrained to the low energy region, where it has had remarkable success, but makes unaffordable the study of the intermediate energy region where resonances appear. In recent years, however, the combination of the information of the chiral Lagrangians, together with the use of nonperturbative schemes, has allowed one to make predictions beyond those of the chiral perturbation expansion. The main idea that has allowed the extension of χPT to higher energies is the inclusion of unitarity in coupled channels. Within the framework of chiral dynamics, the combination of unitarity in coupled channels together with a reordering of the chiral expansion provides a faster convergence and a larger convergence radius of a new chiral expansion, such that the lowest energy resonances are generated within those schemes. A pioneering work along these directions was made in Refs. [6–8] where the Lippmann-Schwinger equation in coupled channels was used to deal with the meson-baryon interaction in the region of the $N^*(1535)$ and $\Lambda(1405)$ resonances. Similar lines, using the Bethe-Salpeter equation in the meson-meson interaction, were followed in Ref. [9] and a more elaborate framework was subsequently developed using the inverse amplitude method (IAM) [10] and the N/D method [11]. The IAM method was also extended to the case of the meson-baryon interaction in Refs. [12,13] where a good reproduction of the Δ resonance was obtained using second order parameters of natural size. The N/D method has also been used for πN scattering [14] and in the K^-N and coupled channels system in Ref. [15]. A review of these unitary methods can be seen in Ref. [16]. The consideration of coupled channels to study meson-baryon interactions at intermediate energies has also been exploited in Refs. [17,18] using the *K*-matrix approach, although not within a chiral context.

The Bethe-Salpeter equation was also used in the study of the meson-baryon interaction in the strangeness $S=-1$ sector in Ref. [19] and in the $S=0$ sector around the $N^*(1535)$ region in Ref. [20]. In this latter work, aimed at determining the $N^*N^*\pi$ coupling, only the vicinity of the resonance was studied and no particular attention was given to the region of lower energies. Subsequently a work along the same lines using the Bethe-Salpeter equation, but considering all the freedom of the chiral constraints, was done in Ref. [21] and a good reproduction of the experimental observables was obtained for the isospin $I=1/2$ sector. Those works considered only states of the meson baryon in the coupled channels and both in Refs. [20] and [21] the $\pi\pi N$ channel was omitted. This channel plays a moderate role in the $I=1/2$ sector [22] but, as we shall see, it plays a crucial role in the $I=3/2$ sector.

Our aim in the present work is to extend the chiral unitary approach to account for the $\pi\pi N$ channel, including simultaneously some other corrections inspired by vector meson dominance (VMD) which finally allows one to have a reasonable description of the meson-baryon interaction up to meson-baryon energies of around 1600 MeV. The $N^*(1535)$ resonance is generated dynamically in this approach and the mass, width, and branching ratios are obtained in fair agreement with the experiment. The phase shifts and inelasticities for πN scattering in that region are also evaluated and good agreement with experiment is also found both in the $I=1/2$ and $I=3/2$ sectors. In addition some trace of the $\Delta(1620)$ is found, linked to the introduction of the $\pi\pi N$ channel, with a pole in the second Riemann sheet with the right energy, albeit a large width.

A side effect of the calculations is that we determine the *S*-wave part of the $\pi N \rightarrow \pi\pi N$ transition amplitude, revising previous determinations mode in Refs. [23,24], and together with the *P*-wave amplitudes previously determined we obtain a good reproduction of the cross sections for these reactions.

*Email address: inoue@ific.uv.es

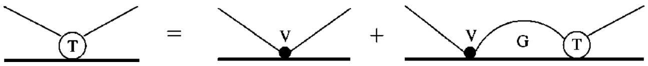

FIG. 1. Diagrammatic representation of the Bethe-Salpeter equation.

II. πN SCATTERING IN A TWO-BODY COUPLED CHANNEL MODEL

A. Basic two-body model

In this section we study the meson-baryon scattering in S-wave in the strangeness $S=0$ sector. We shall make use of the Bethe-Salpeter equation in coupled channels considering states of a meson of the 0^- octet and a baryon of the $1/2^+$ octet, as required by the SU(3) chiral formalism. For total zero charge we have six channels $\pi^- p$, $\pi^0 n$, ηn, $K^+\Sigma^-$, $K^0\Sigma^0$, and $K^0\Lambda$.

The Bethe-Salpeter equation of the scattering amplitudes T is given by

$$T=V+VGT, \tag{1}$$

where V and G are the kernel (potential) and the product of the meson and baryon propagators, respectively. The diagrammatic expression is shown in Fig. 1. Following Ref. [19] we take the kernel of the Bethe-Salpeter equation from the lowest order chiral Lagrangian involving mesons and baryons, and the transition potentials between our six channels are given by

$$V_{ij}=-C_{ij}\frac{1}{4f^2}\overline{u}(p')\gamma^{\mu}u(p)(k_{\mu}+k'_{\mu}) \tag{2}$$

with the initial (final) baryon spinor $u(p)[u(p')]$ and the initial (final) meson momentum $k(k')$. The coefficients C_{ij}, reflecting the SU(3) symmetry of the problem, are shown in Table I.

We are interested in the value of the T-matrix element for the on-shell meson-baryon systems at a certain center of mass energy $\sqrt{s}$ or $P\equiv p+k=(\sqrt{s},0,0,0)$, and we express it as $T(\sqrt{s})$. Yet, in the diagrammatic expression of the Bethe-Salpeter equation, Fig. 1, one can see that the V and T matrices in the second diagram on the right hand side can be (half) off shell, since the Bethe-Salpeter equation is an integral equation. However, it was shown in Ref. [19] that the off-shell part of these matrices in the loops could be incorporated into a renormalization of the lowest order Lagrangian and hence only the on-shell parts are needed. Thus, they factorize out of the integral and the original Bethe-Salpeter equation is then reduced to an algebraic equation. The standard approximations used in heavy baryon chiral perturbation theory were done in Ref. [19] to reach this conclusion. An independent proof is done in Ref. [15] where the N/D method is used in connection with dispersion relations which select the imaginary part of the loop functions and hence on-shell magnitudes. There it is concluded that the on-shell factorization is exact if one neglects the left hand cut, which, as also discussed there, is practically negligible in this process. With the on-shell factorization, the Bethe-Salpeter equation is easily solved with the solution in matrix form,

$$T(\sqrt{s})=[V(\sqrt{s})^{-1}-G(\sqrt{s})]^{-1}$$

or

$$T(\sqrt{s})^{-1}=V(\sqrt{s})^{-1}-G(\sqrt{s}), \tag{3}$$

where the function $G(\sqrt{s})$ is a diagonal matrix representing the loop integral of a meson and a baryon. The ith element is thus expressed as

$$G_i(P)=i\int\frac{d^4q}{(2\pi)^4}\frac{2M_i}{(P-q)^2-M_i^2+i\epsilon}\frac{1}{q^2-m_i^2+i\epsilon} \tag{4}$$

with the baryon mass M_i and meson mass m_i.

The explicit evaluation of Eq. (2) gives

$$V_{ij}(\sqrt{s})=-C_{ij}\frac{1}{4f_if_j}(2\sqrt{s}-M_i-M_j)\times\sqrt{\frac{M_i+E_i(\sqrt{s})}{2M_i}}\sqrt{\frac{M_j+E_j(\sqrt{s})}{2M_j}}, \tag{5}$$

where E_i (E_j) is the energy of the incoming (outgoing) baryon. Note that we introduce the different weak decay constants for each meson. We use the values $f_\pi=93$ MeV, $f_K=1.22f_\pi$, and $f_\eta=1.3f_\pi$ taken from χPT [1].

The meson-baryon loop function of Eq. (4) using the dimensional regularization is given by

$$\begin{aligned}\mathrm{G}_i(\sqrt{s})=\frac{2M_i}{(4\pi)^2}\Bigg\{&a_i(\mu)+\ln\frac{m_i^2}{\mu^2}+\frac{M_i^2-m_i^2+s}{2s}\ln\frac{M_i^2}{m_i^2}\\&+\frac{Q_i(\sqrt{s})}{\sqrt{s}}[\ln(s-(M_i^2-m_i^2)+2\sqrt{s}Q_i(\sqrt{s}))\\&+\ln(s+(M_i^2-m_i^2)+2\sqrt{s}Q_i(\sqrt{s}))\\&-\ln(-s+(M_i^2-m_i^2)+2\sqrt{s}Q_i(\sqrt{s}))\\&-\ln(-s-(M_i^2-m_i^2)+2\sqrt{s}Q_i(\sqrt{s}))]\Bigg\},\end{aligned} \tag{6}$$

TABLE I. C_{ij} coefficients in the potential ($C_{ij}=C_{ji}$).

	$K^+\Sigma^-$	$K^0\Sigma^0$	$K^0\Lambda$	$\pi^- p$	$\pi^0 n$	ηn
$K^+\Sigma^-$	1	$-\sqrt{2}$	0	0	$-\frac{1}{\sqrt{2}}$	$-\sqrt{\frac{3}{2}}$
$K^0\Sigma^0$		0	0	$-\frac{1}{\sqrt{2}}$	$-\frac{1}{2}$	$\frac{\sqrt{3}}{2}$
$K^0\Lambda$			0	$-\sqrt{\frac{3}{2}}$	$\frac{\sqrt{3}}{2}$	$-\frac{3}{2}$
$\pi^- p$				1	$-\sqrt{2}$	0
$\pi^0 n$					0	0
ηn						0

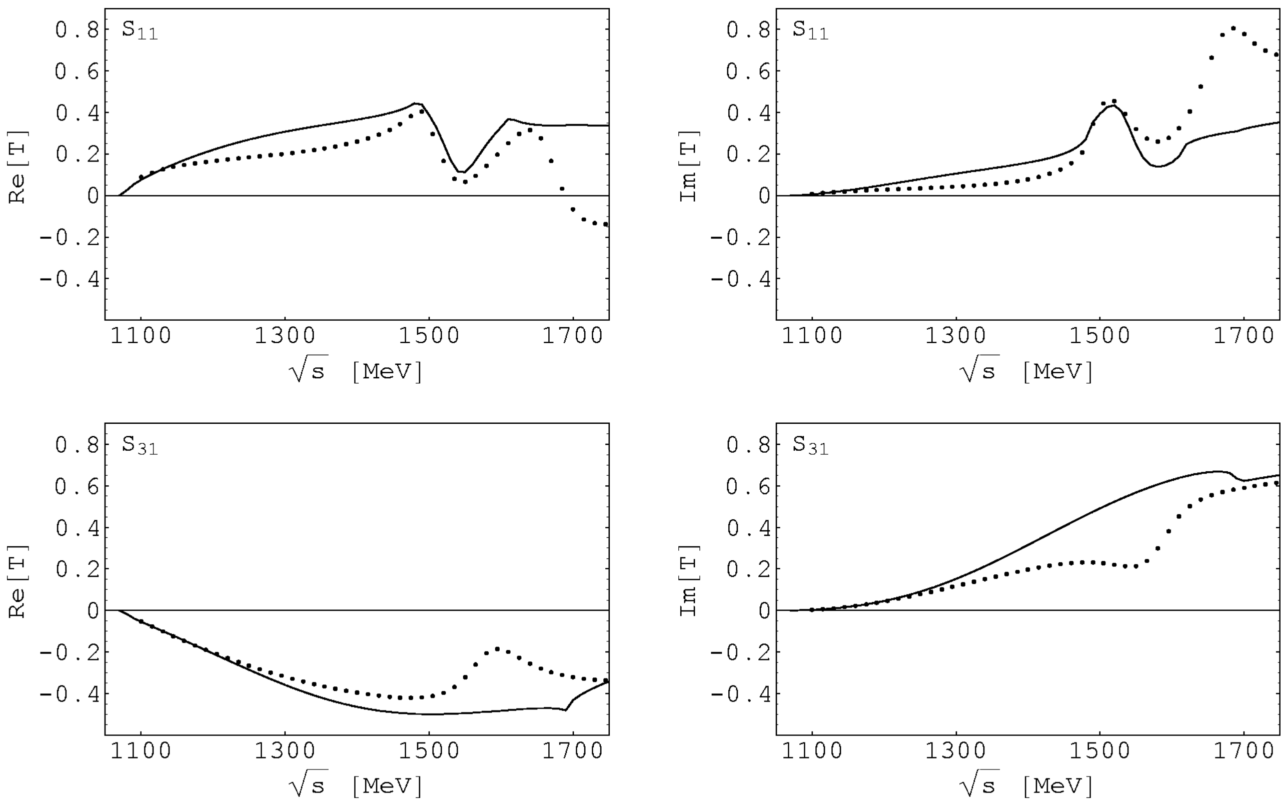

FIG. 2. Scattering amplitude for the S_{11} and S_{31} πN partial waves. The continuous (dotted) lines correspond to the calculations (data analysis, Ref. [26]).

where $Q_i(\sqrt{s})$ is the on-shell center of mass momentum of the ith meson-baryon system. The first terms $a_i(\mu)$ are real constants and stand for the finite contribution of the counterterms. We treat these $a_i(\mu)$ as unknown parameters and determine them from fits to the data. Note that the imaginary part of the above loop function is

$$\mathrm{Im}[G_i(\sqrt{s})] = -\frac{M_i Q_i(\sqrt{s})}{4\pi\sqrt{s}}, \tag{7}$$

which by means of Eq. (3) can be recast as

$$\mathrm{Im}[T_{ij}(\sqrt{s})] = -T_{ik}(\sqrt{s})\frac{M_k Q_k(\sqrt{s})}{4\pi\sqrt{s}}T^*_{kj}(\sqrt{s})$$

or

$$\mathrm{Im}[T^{-1}(\sqrt{s})]_{ij} = \delta_{ij}\frac{M_i Q_i(\sqrt{s})}{4\pi\sqrt{s}}, \tag{8}$$

which express the unitarity condition in the present normalization [25].

In order to keep isospin symmetry for the case in which the masses of the particles in the same multiplet are equal, we choose $a_i(\mu)$ to be the same for the states belonging to the same isospin multiplet. Hence we have four subtraction constants $a_{\pi N}(\mu)$, $a_{\eta N}(\mu)$, $a_{K\Lambda}(\mu)$, and $a_{K\Sigma}(\mu)$. A best fit to the data with Eq. (3) leads us to the following values of these parameters:

$$\mu = 1200\ \text{MeV}, \quad a_{\pi N}(\mu) = 2.0, \quad a_{\eta N}(\mu) = 0.2,$$
$$a_{K\Lambda}(\mu) = 1.6, \quad a_{K\Sigma}(\mu) = -2.8. \tag{9}$$

The $G(\sqrt{s})_i$ obtained with this set of parameters are essentially the same as those obtained in Ref. [20] where the regularization was done using a three-momentum cutoff ($|\vec{q}| < 1$ GeV).

The resulting *T*-matrix elements of S_{11} (isospin 1/2) and S_{31} (isospin 3/2) πN elastic scattering are shown in Fig. 2. In these graphs we plot the quantity

$$-\sqrt{\frac{M_i Q_i(\sqrt{s})}{4\pi\sqrt{s}}}\sqrt{\frac{M_j Q_j(\sqrt{s})}{4\pi\sqrt{s}}}T_{ij}(\sqrt{s}) \tag{10}$$

in order to compare with the data of the Center of Nuclear Study analysis [26]. We find a qualitative agreement with the data in the energy range from threshold to 1600 MeV. In the figure of the experimental analysis one can see the manifestation of the resonances $N^*(1535)$, $N^*(1650)$ in the S_{11} amplitude and $\Delta(1620)$ in the S_{31} one. The calculated S_{11} amplitude also exhibits a resonance structure around 1535 MeV. The generation of this resonance is common to all the unitary chiral approaches [6,20,21]. In Sec. IV, after we include new elements in the theory, we shall investigate this resonance by searching for poles in the second Riemann sheet of the complex plane.

At energies beyond 1600 MeV, the calculated amplitudes are qualitatively different from the data, and the $N^*(1650)$

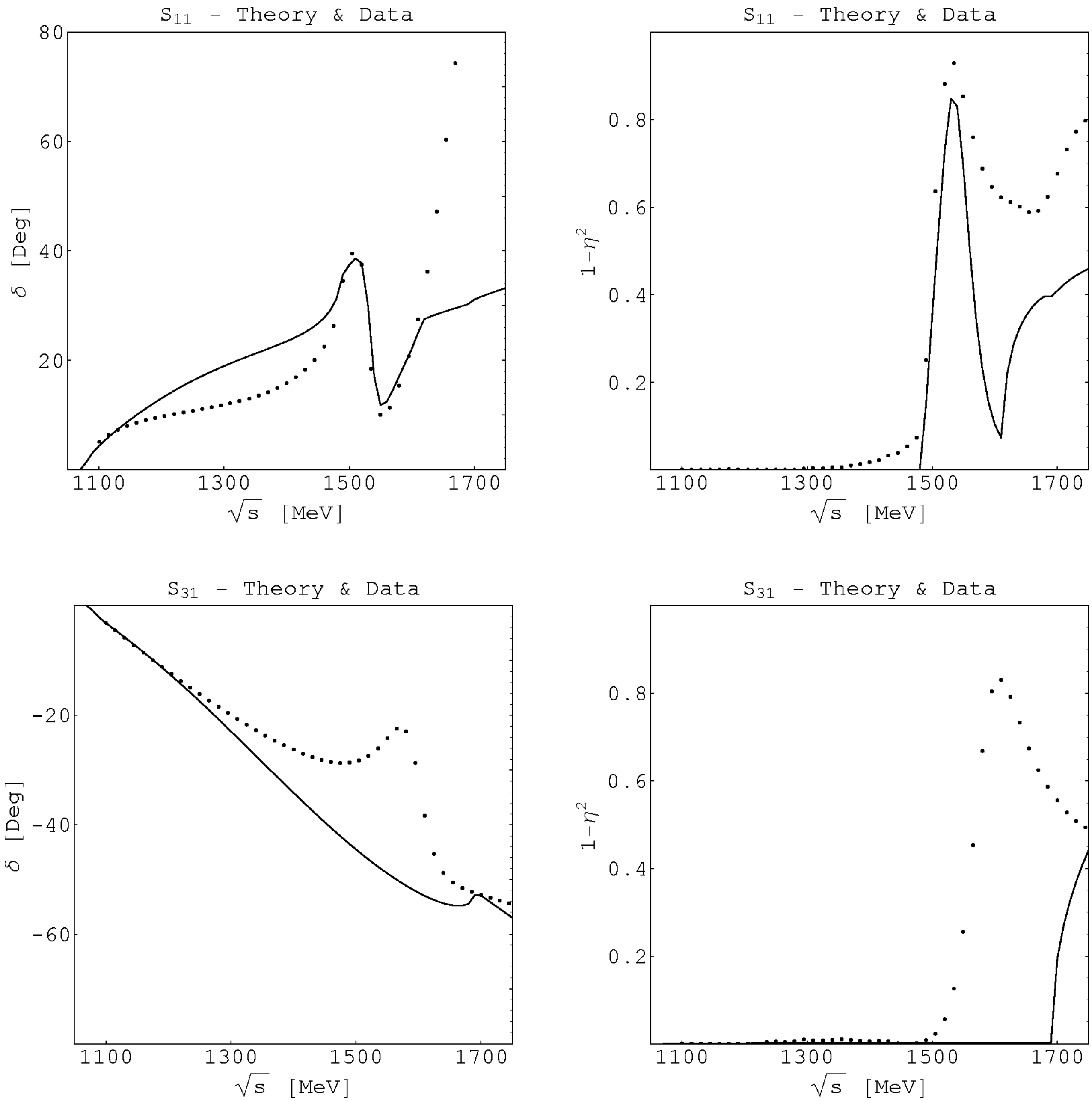

FIG. 3. Phase shifts and inelasticities for S_{11} and S_{31} πN scattering. The continuous (dotted) lines correspond to the calculations (data analysis, Ref. [26]).

and $\Delta(1620)$ do not show up. According to the philosophy that the resonances obtained using the lowest order Lagrangian and the present unitary scheme are simply meson-baryon scattering resonances (qualifying for quasibound meson-baryon states [16]), the nongeneration of a particular resonance would indicate that it is mostly a genuine state (approximately a $3q$ system). However, such resonances could be also obtained in a unitary approach provided one used information related to this resonance which would be incorporated in the higher order Lagrangians. For the case of the meson-meson interaction it is known [27] that the $O(p^4)$ Lagrangian is saturated by the exchange of vector meson resonances, which are not generated in the Bethe-Salpeter approach of Ref. [9]. Actually, in Ref. [21] the $N^*(1650)$ resonance is also reproduced by introducing counterterms which effectively account for higher order corrections, much in the way as the (genuine) ρ resonance was reproduced in the study of the meson-meson scattering in Refs. [28,29]. As quoted before, the agreement below 1600 MeV is only qualitative. Indeed, both the real and imaginary parts of the S_{11} amplitude are somewhat overestimated in the theory, and this is also the case for the S_{31} amplitude where the theoretical imaginary part clearly overestimates the experimental one.

The phase shifts and inelasticities obtained are shown in Fig. 3. In the phase-shifts graph we can see again the qualitative agreement at energies below 1600 MeV. On the other hand, the inelasticities are not reproduced below the first open meson-baryon threshold. In this two-body model the

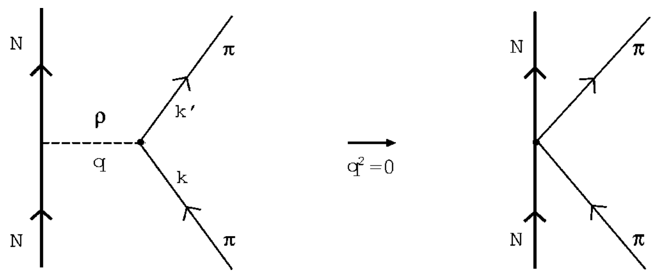

FIG. 4. The mechanism of $\pi N \to \pi N$ interaction in the vector meson dominance hypothesis.

threshold of inelastic scattering for the S_{11} case is the ηn threshold which appears at 1487 MeV. Below this energy, the calculated inelasticities are zero and do not agree with the data. This situation is even clearer in the S_{31} case. The threshold of inelastic scattering is in this case the $K\Sigma$ threshold which appears at 1690 MeV. The big inelasticities observed in the data, below that energy, are not reproduced in the present two-body approach. The only inelastic channel opened below that energy is the $\pi\pi N$ channel, and the experimental data is telling us that the influence of this channel on the S_{31} amplitude should be very important. We will include the $\pi\pi N$ channel in the next section.

B. Improved two-body model

The vector meson dominance (VMD) hypothesis is phenomenologically very successful. In this hypothesis, the meson-baryon interaction is provided by vector meson exchange. For example, the $\pi N \to \pi N$ process is described by ρ meson exchange in the t channel, as shown in Fig. 4. It is interesting to note that the result from ρ exchange provides the amplitude obtained from the lowest order chiral Lagrangian. For example, in the case of $\pi^- p \to \pi^- p$, ρ exchange in the t channel gives (see Ref. [30] for the ρNN coupling within the VMD hypothesis)

$$i\frac{m_\rho G_v}{2f^2}\gamma^\mu \epsilon_\mu \frac{i}{q^2-m_\rho^2} i\frac{m_\rho G_v}{f^2}\epsilon^\nu (k+k')_\nu \bigg|_{q^2=0} = -i\frac{1}{4f^2}\gamma^\mu (k+k')_\mu, \tag{11}$$

which follows from the relation $G_v^2/f^2 = 1/2$, which is a result of the VMD hypothesis. This indicates that the lowest order chiral Lagrangian is an effective manifestation of the VMD mechanism in the vector field representation of the vector mesons. According to this consideration, we introduce in the chiral coefficient a correction to account for the dependence on the momentum transfer of the vector meson propagator. Thus we replace

$$C_{ij} \to \tilde{C}_{ij} \equiv C_{ij} \times \int \frac{d\hat{k}'}{4\pi}\frac{-m_v^2}{(k'-k)^2-m_v^2}$$

at

$$\sqrt{s} > \sqrt{s_{ij}^0}, \tag{12}$$

where $\sqrt{s_{ij}^0}$ is the energy where the integral of Eq. (12) is unity, and which appears between the thresholds of the two i,j channels. At very low energies where χPT is used, this correction is negligible but this is not the case at the intermediate energies studied here. For example, the correction for the $\pi^- p \to \pi^- p$ element is calculated as

$$\int \frac{d\hat{k}'}{4\pi}\frac{-m_\rho^2}{(k'-k)^2-m_\rho^2} = \frac{m_\rho^2}{4kk'}\ln\frac{m_\rho^2+2k^0k'^0+2kk'-m_\pi^2-m_\pi^2}{m_\rho^2+2k^0k'^0-2kk'-m_\pi^2-m_\pi^2} \tag{13}$$

with $m_\rho = 770$ [MeV], and is shown in at the left in Fig. 5. One can see that the ρ meson tail reduces the coefficient by about 25% at energies around 1500 MeV. Similarly, for the strangeness exchanging process, we consider K^* exchange in the t channel. For example, the correction of $\pi^- p \to K^0 \Lambda$ is calculated with $m_{K^*} = 892$ MeV and shown in at the left in Fig. 5.

With this correction, after retuning the subtraction constants $a_i(\mu)$, we obtain the T matrix shown in Fig. 6. As we can see, the problem of the previous overestimation is nearly solved. Especially, a drastic improvement is achieved for the S_{31} amplitude. The phase shifts are better reproduced now as shown in Fig. 7. These results show that the correction of Eq. (12) is important and leads to improved results with respect to the plain use of the standard lowest order chiral Lagrang-

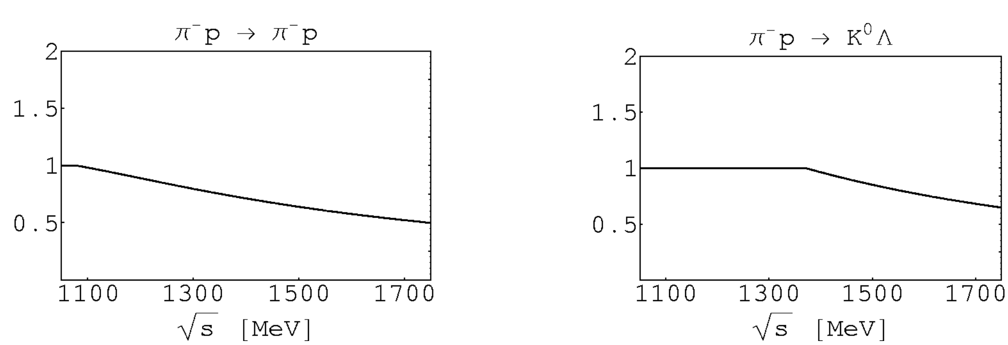

FIG. 5. Correction factors of the chiral coefficient.

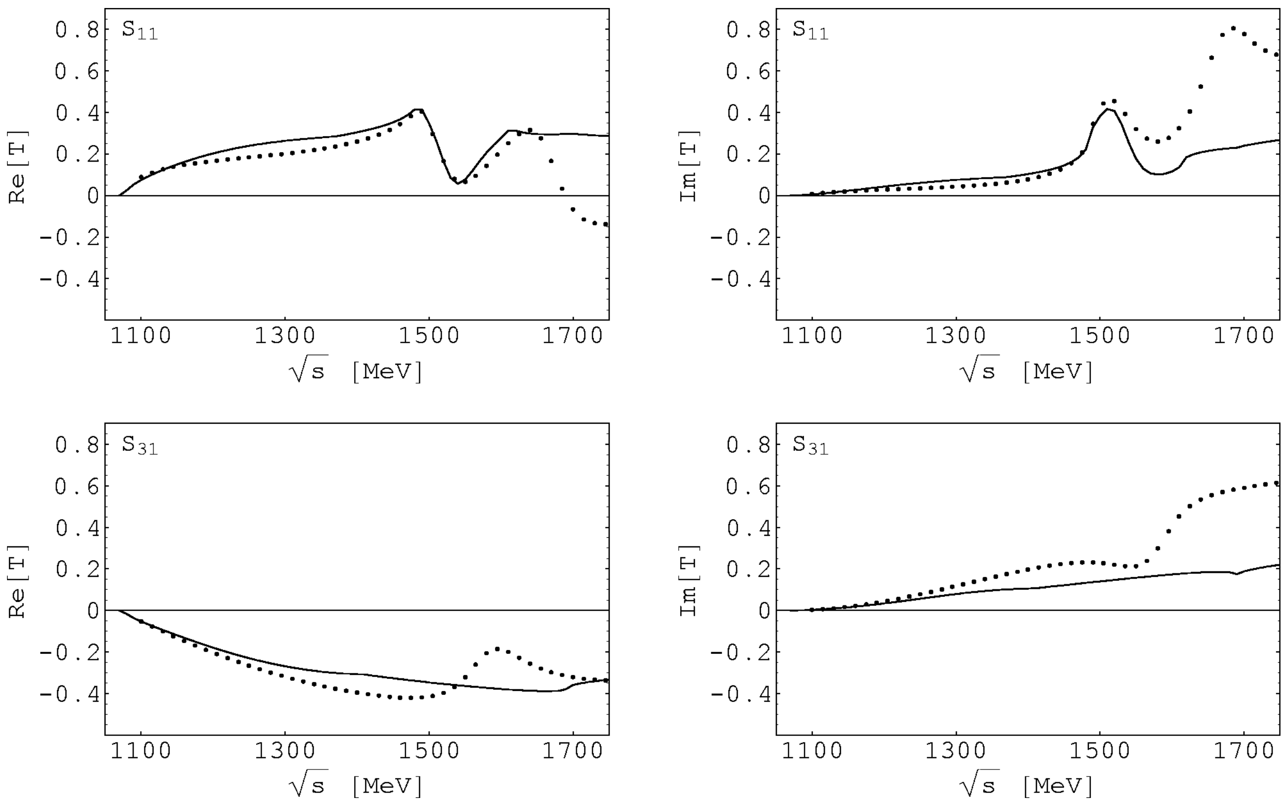

FIG. 6. Scattering amplitudes for the S_{11} and S_{31} πN partial waves with the improved C_{ij}. The continuous (dotted) lines correspond to the calculations (data analysis, Ref. [26]).

ian. In the following sections, we employ this modified coefficient. The calculated inelasticities with this coefficient are almost the same as before and show the lack of some important channels. We come back to this problem in the next section.

III. πN SCATTERING IN A TWO–THREE-BODY COUPLED CHANNEL MODEL

In this section, we extend our model to include the $\pi\pi N$ channels. The cross sections of the $\pi N \to \pi\pi N$ scattering are known experimentally and they are sizeable compared with the two-body cross sections. In this paper, we include only the transition potential between πN and $\pi\pi N$ and disregard the coupling between the $\{K\Sigma, K\Lambda, \eta n, \pi\pi N\}$ states and the $\pi\pi N$. This is a simplification forced by the ignorance of such couplings, but the larger mass of these states with respect to πN, and the fact that we are talking about corrections, makes this simplification justifiable.

A. $\pi N \to \pi\pi N$ process

In the isospin formalism, the $\pi N \to \pi\pi N$ transition amplitudes can be classified by the total isospin I and the isospin of the final two pions $I_{\pi\pi}$, and the corresponding amplitudes are written as $A_{2II_{\pi\pi}}$. The amplitudes of the physical processes are expressed in terms of the following four independent isospin amplitudes:

$$A_{11} = a_{11}\, \chi_f^\dagger \vec{\sigma}\cdot(\vec{k}_1' - \vec{k}_2')\chi_i, \quad A_{31} = a_{31}\, \chi_f^\dagger \vec{\sigma}\cdot(\vec{k}_1' - \vec{k}_2')\chi_i,$$

$$A_{10} = a_{10}\, \chi_f^\dagger \vec{\sigma}\cdot\vec{k}\chi_i, \quad A_{32} = a_{32}\, \chi_f^\dagger \vec{\sigma}\cdot\vec{k}\chi_i, \tag{14}$$

where χ_i and χ_f are spinors for the initial and final nucleons, and $\vec{k}$, $\vec{k}_1'$, and $\vec{k}_2'$ are the momenta of the pions depicted in Fig. 8. Among these amplitudes, the upper two amplitudes which have $I_{\pi\pi}=1$ correspond to transitions from πN in an S wave, while the lower two amplitudes correspond to the transition in P wave.

These amplitudes have been extracted by analyzing the experimental cross sections. In Ref. [23], the data from threshold to 1470 MeV are analyzed. The reduced amplitudes a_{ij} are assumed to be constant except for a_{10} which has a resonance behavior due to a coupling to the Roper resonance, $P_{11}(1440)$,

$$a_{10}(\sqrt{s}) = a_{10}' \frac{M - \sqrt{s_{th}}}{M - \sqrt{s} - i\Gamma/2\,(\sqrt{s} - \sqrt{s_{th}}/M - \sqrt{s_{th}})^2}, \tag{15}$$

where $\sqrt{s_{th}} \sim 1213$ MeV is the threshold energy. The reduced amplitudes obtained are

$$a_{11} = 10.61 \pm 0.62\,[m_\pi^{-3}], \quad a_{31} = -6.02 \pm 0.31\,[m_\pi^{-3}],$$

$$a_{10}' = 6.63 \pm 0.21\,[m_\pi^{-3}], \quad a_{32} = 2.75 \pm 0.13\,[m_\pi^{-3}] \tag{16}$$

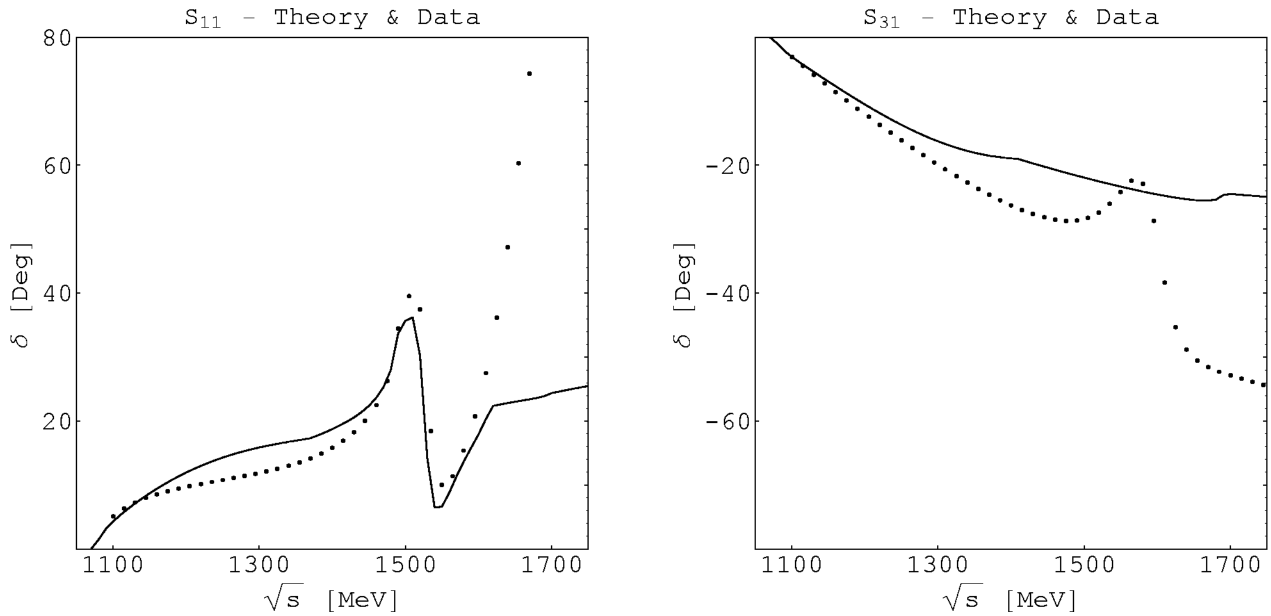

FIG. 7. Phase shifts for S_{11} and S_{31} πN scattering with the improved C_{ij}. The continuous (dotted) lines correspond to the calculations (data analysis, Ref. [26]).

with $M=1416\pm14$ MeV and $\Gamma=287\pm43$ MeV. In Ref. [24], the data close to threshold, including newer data with respect to Ref. [23], are analyzed. In this case the reduced amplitudes are assumed to depend linearly on the center of mass energy. The reduced amplitudes

$$a_{11}=3.3\pm0.8+(0.9\pm2.0)(\sqrt{s}-\sqrt{s_{th}})/m_\pi \;\; [m_\pi^{-3}], \tag{17}$$

$$a_{31}=-5.0\pm2.2+(15.0\pm4.2)(\sqrt{s}-\sqrt{s_{th}})/m_\pi \;\; [m_\pi^{-3}], \tag{18}$$

$$a_{10}=6.55\pm0.16+(10.4\pm0.8)(\sqrt{s}-\sqrt{s_{th}})/m_\pi \;\; [m_\pi^{-3}], \tag{19}$$

$$a_{32}=2.07\pm0.10+(1.98\pm0.33)(\sqrt{s}-\sqrt{s_{th}})/m_\pi \;\; [m_\pi^{-3}] \tag{20}$$

are obtained.

We plot both empirical reduced amplitudes in Fig. 9. One can see that the extracted amplitudes of *S* wave πN are very different in both analyses, while those of *P* wave πN agree quite well. These discrepancies reflect the difficulties of determining the amplitudes of the *S* wave πN from $(\pi,2\pi)$ cross section data, which look quite natural since most of the processes are dominated by the transition from *P* wave.

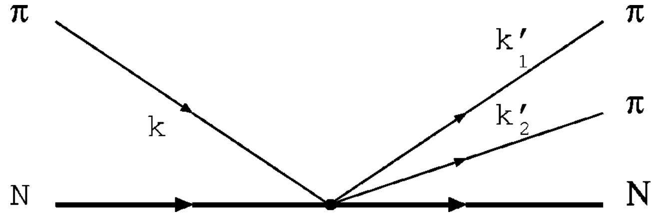

FIG. 8. $\pi N\rightarrow\pi\pi N$ process.

Therefore, in this paper, we leave free the *S*-wave πN amplitudes, $a_{11}(\sqrt{s})$ and $a_{31}(\sqrt{s})$, and determine them through the present study so that they are compatible with the data of $\pi N\rightarrow\pi N$ elastic scattering.

B. The model including the $\pi\pi N$ channel

We consider the Bethe-Salpeter equation for the scattering matrix, Eq. (1), with the eight coupled channels including $\pi\pi N$, namely, $\pi^- p$, $\pi^0 n$, ηn, $K^+\Sigma^-$, $K^0\Sigma^0$, $K^0\Lambda$, $\pi^0\pi^- p$, and $\pi^+\pi^- n$. We do not include the $\pi^0\pi^0 n$ channel because it does not couple to the *S* wave πN state.

The potentials of the $\pi N\leftrightarrow\pi\pi N$ transitions are written as

$$V_{\pi^- p,\pi^0\pi^- p}=\left[\frac{\sqrt{2}}{3}v_{11}+\frac{\sqrt{2}}{6}v_{31}\right]\chi_f^\dagger\vec{\sigma}\cdot(\vec{k}_1'-\vec{k}_2')\chi_i - \frac{\sqrt{10}}{10}v_{32}\chi_f^\dagger\vec{\sigma}\cdot\vec{k}\chi_i, \tag{21}$$

$$V_{\pi^- p,\pi^+\pi^- n}=\left[\frac{1}{3}v_{11}-\frac{1}{3}v_{31}\right]\chi_f^\dagger\vec{\sigma}\cdot(\vec{k}_1'-\vec{k}_2')\chi_i + \left[\frac{\sqrt{2}}{3}v_{10}-\frac{\sqrt{5}}{15}v_{32}\right]\chi_f^\dagger\vec{\sigma}\cdot\vec{k}\chi_i, \tag{22}$$

$$V_{\pi^0 n,\pi^0\pi^- p}=\left[-\frac{1}{3}v_{11}+\frac{1}{3}v_{31}\right]\chi_f^\dagger\vec{\sigma}\cdot(\vec{k}_1'-\vec{k}_2')\chi_i - \frac{\sqrt{5}}{5}v_{32}\chi_f^\dagger\vec{\sigma}\cdot\vec{k}\chi_i, \tag{23}$$

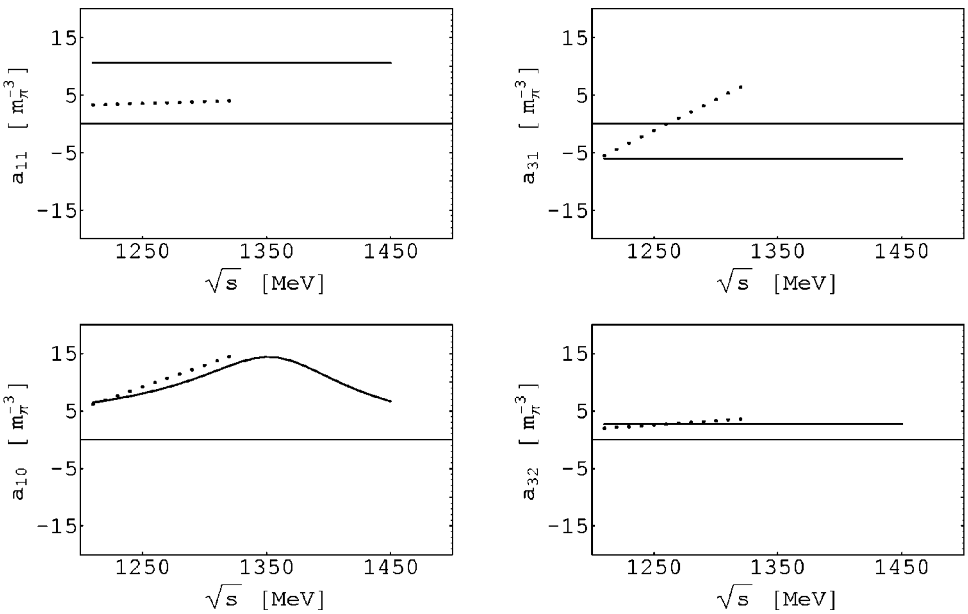

FIG. 9. Empirical amplitudes of the $\pi N \to \pi\pi N$ transition. The continuous lines and dotted lines correspond to the amplitudes of Refs. [23] and [24], respectively. The absolute value is plotted for $a_{10}(\sqrt{s})$ of Ref. [23].

$$V_{\pi^0 n, \pi^+\pi^- n} = \left[-\frac{\sqrt{2}}{6} v_{11} - \frac{\sqrt{2}}{3} v_{31} \right] \chi_f^\dagger \vec{\sigma} \cdot (\vec{k}_1' - \vec{k}_2') \chi_i + \left[-\frac{1}{3} v_{10} - \frac{\sqrt{10}}{15} v_{32} \right] \chi_f^\dagger \vec{\sigma} \cdot \vec{k} \chi_i \tag{24}$$

in terms of the reduced potentials $v_{11}(\sqrt{s})$, $v_{31}(\sqrt{s})$, $v_{10}(\sqrt{s})$, and $v_{32}(\sqrt{s})$, which correspond to the reduced amplitudes $a_{11}(\sqrt{s})$, $a_{31}(\sqrt{s})$, $a_{10}(\sqrt{s})$, and $a_{32}(\sqrt{s})$, respectively, after solving the Bethe-Salpeter equation with all the channels. Note that, in our formalism, π^+ corresponds to the $-|I=1, I_z=1\rangle$ state. The terms of $v_{10}(\sqrt{s})$ and $v_{32}(\sqrt{s})$ do not contribute in the present *S*-wave scattering.

For the $\pi\pi N$ state, we introduce the two-loop integral corresponding to Fig. 10,

$$\tilde{G}(P) = i^2 \int \frac{d^4 q_1}{(2\pi)^4} \int \frac{d^4 q_2}{(2\pi)^4} (\vec{q}_1 - \vec{q}_2)^2 \times \frac{2M_N}{(P - q_1 - q_2)^2 - M_N^2 + i\epsilon} \frac{1}{q_1^2 - m_\pi^2 + i\epsilon} \times \frac{1}{q_2^2 - m_\pi^2 + i\epsilon}, \tag{25}$$

which includes the vertex structure for the factorization. Its imaginary part is given by

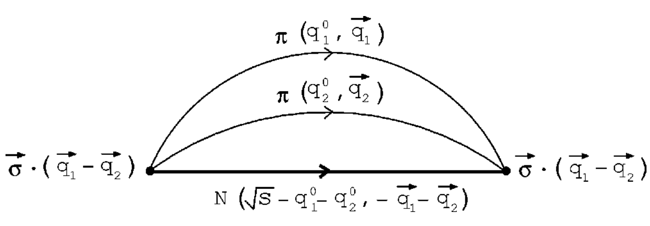

FIG. 10. Loop for the $\pi\pi N$ state.

$$\mathrm{Im}[\tilde{G}(\sqrt{s})] = -\frac{M_N}{4(2\pi)^3} \int d\omega_1 \int d\omega_2 \times [M_N^2 + 2q_1(\omega_1)^2 + 2q_2(\omega_2)^2 - (\sqrt{s} - \omega_1 - \omega_2)^2] \theta(1 - A^2), \tag{26}$$

where

$$A = \frac{(\sqrt{s} - \omega_1 - \omega_2)^2 - M_N^2 - q_1(\omega_1)^2 - q_2(\omega_2)^2}{2q_1(\omega_1) q_2(\omega_2)} \tag{27}$$

with $q_i(\omega_i) = \sqrt{\omega_i^2 - m_\pi^2}$. This imaginary part, reflecting the phase space for the intermediate $\pi\pi N$ system, is shown in Fig. 11. On the other hand, the real part of $\tilde{G}(\sqrt{s})$, in the renormalized model, is not fixed. In a dispersion relation, given the fact that $\mathrm{Im}[\tilde{G}(\sqrt{s})] \times (\sqrt{s})^{-n}$ goes to zero for $n \geqslant 6$, we would need to do six subtractions, and, in this paper, we treat it as a free function and look for reasonable values consistent with the experiment.

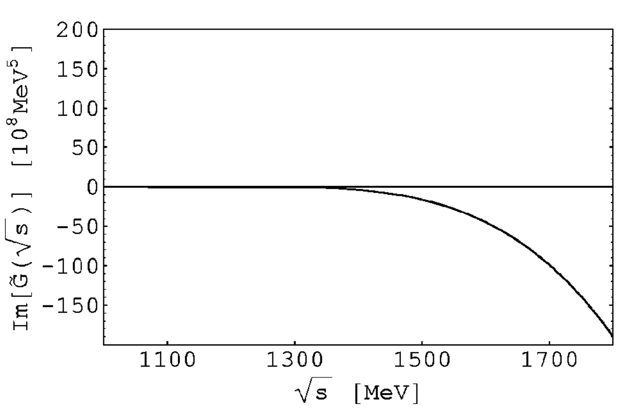

FIG. 11. Imaginary part of $\tilde{G}(\sqrt{s})$.

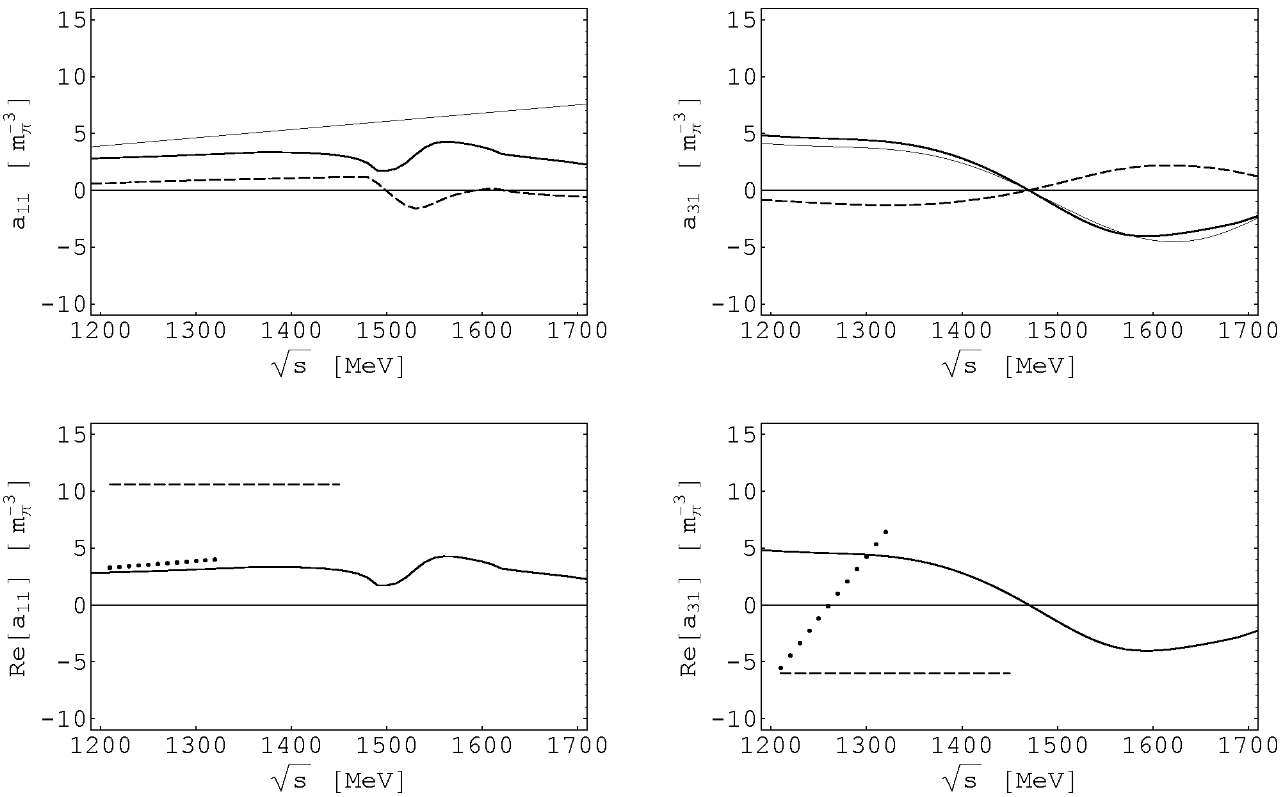

FIG. 12. The *S*-wave $\pi N \leftrightarrow \pi\pi N$ amplitudes $a_{11}(\sqrt{s})$ and $a_{31}(\sqrt{s})$. Upper figures in the panel: the thin lines are the potential $v_{ij}(\sqrt{s})$, the solid lines are $\mathrm{Re}[a_{ij}(\sqrt{s})]$, and the dashed lines are $\mathrm{Im}[a_{ij}]$. Lower figures in the panel: the calculated $\mathrm{Re}[a_{ij}]$(solid) are compared with Refs. [23] (dashed) and [24] (dotted lines).

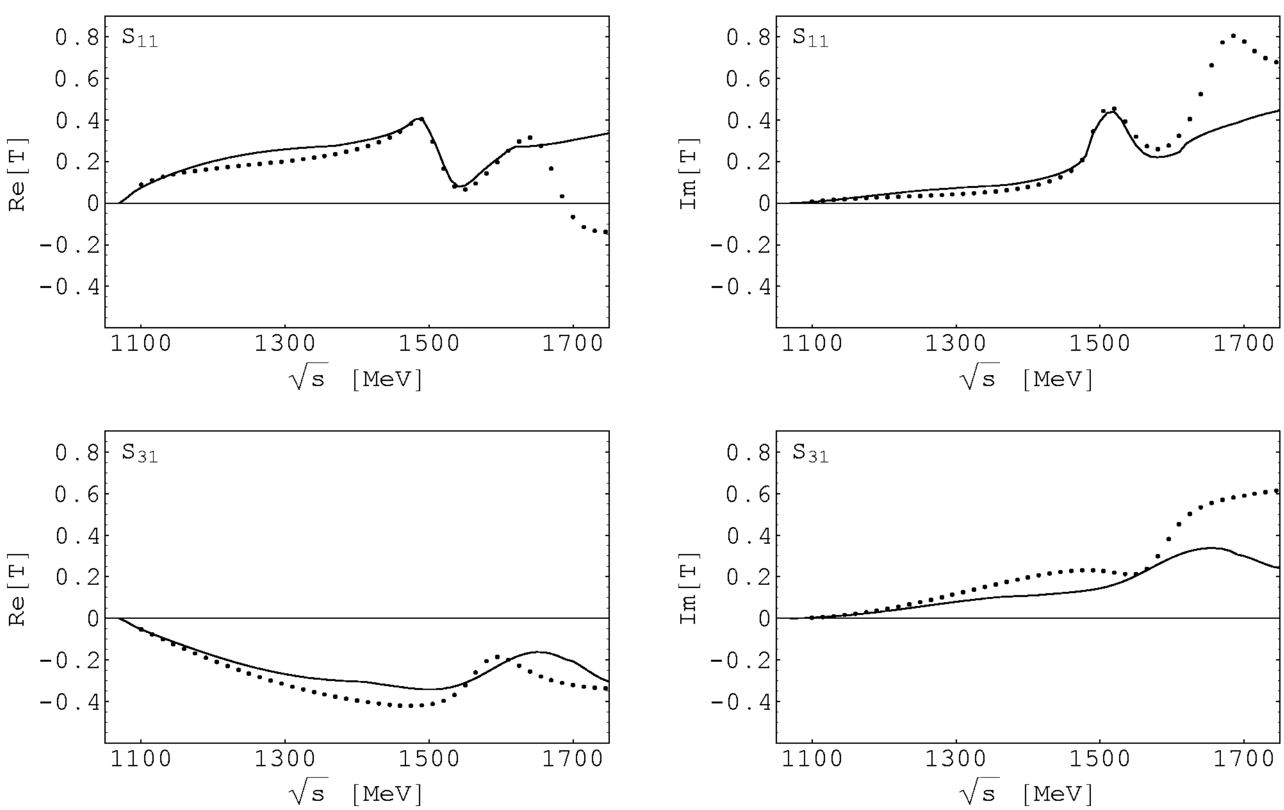

FIG. 13. Scattering amplitudes for the S_{11} and S_{31} πN partial waves with $\pi\pi N$ channels. The continuous (dotted) lines correspond to the calculations (data analysis, Ref. [26]).

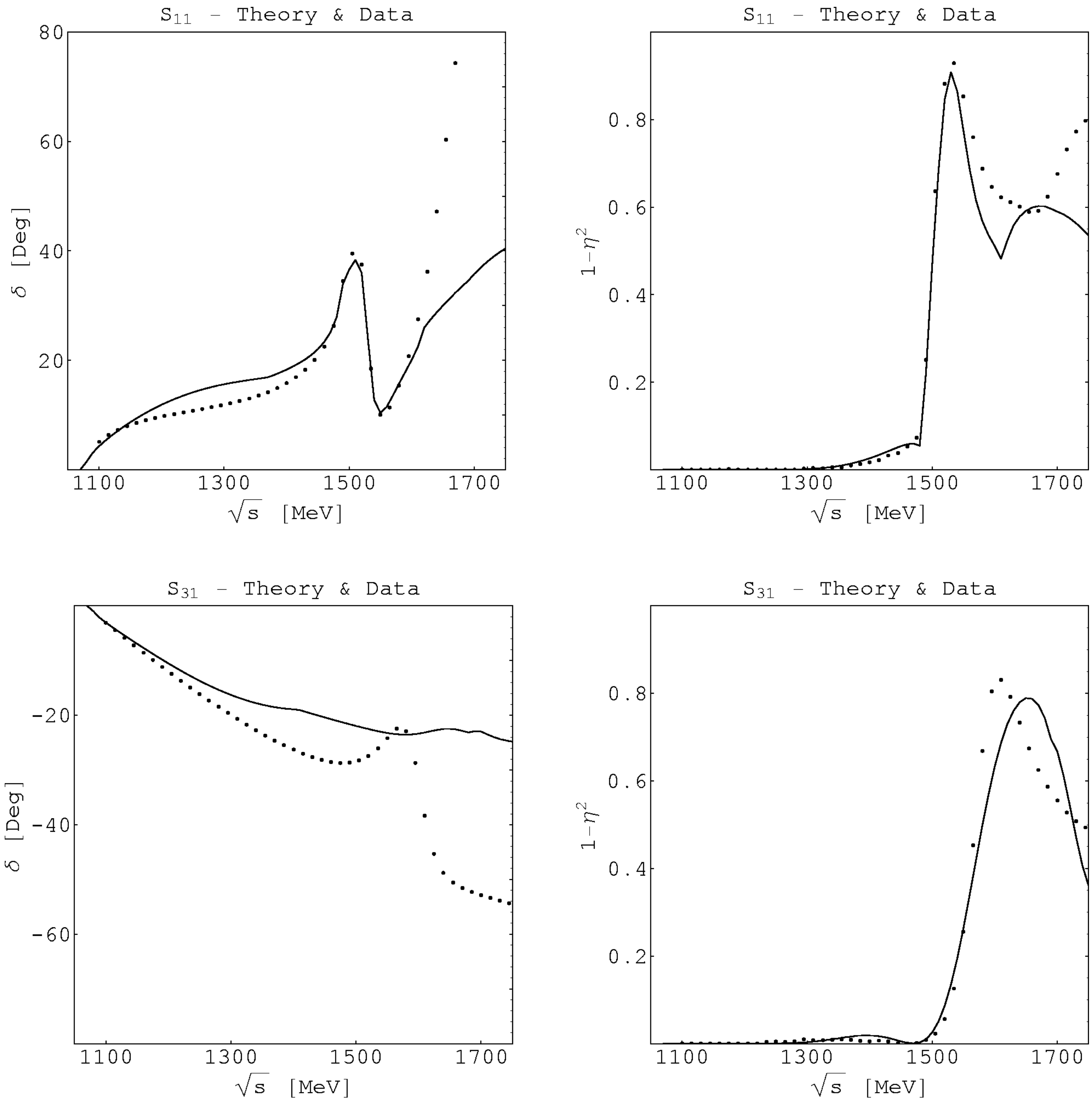

FIG. 14. Phase shifts and inelasticities of S_{11} and S_{31} πN scattering with $\pi\pi N$ channels. The continuous (dotted) lines correspond to the calculations (data analysis, Ref. [26]).

C. Final results

By varying the potentials $v_{11}(\sqrt{s})$ and $v_{31}(\sqrt{s})$, and the subtraction constants $a_i(\mu)$ and $\mathrm{Re}[\tilde{G}(\sqrt{s})]$, we try to reproduce the experimental elastic πN T matrix and also the $\pi N \to \pi\pi N$ cross sections. For the $v_{11}(\sqrt{s})$ and $v_{31}(\sqrt{s})$ functions we employ a real polynomial function, and for $\mathrm{Re}[\tilde{G}(\sqrt{s})]$ we test several types of functions.

The subtraction parameters $a_i(\mu)$ for the meson-baryon loop functions that we obtain in the new fit to the data are

$$\mu = 1200 \ \text{MeV}, \quad a_{\pi N}(\mu) = 2.0, \quad a_{\eta N}(\mu) = 0.1,$$

$$a_{K\Lambda}(\mu) = 1.5, \quad a_{K\Sigma}(\mu) = -2.8, \tag{28}$$

which are a little changed from the previous values omitting the $\pi\pi N$ channels. For $\mathrm{Re}[\tilde{G}(\sqrt{s})]$, we find that the best results are obtained with functions compatible with zero, hence we take $\mathrm{Re}[\tilde{G}(\sqrt{s})] = 0$ in what follows. This result is similar to the one found in Ref. [31] where the real part of the three pion loop forming ϕ decay was also found to be negligibly small.

Figure 12 shows the functions $a_{11}(\sqrt{s})$ and $a_{31}(\sqrt{s})$ determined in this study. In the upper two graphs, the potentials $v_{11}(\sqrt{s})[v_{31}(\sqrt{s})]$ and the amplitudes $a_{11}(\sqrt{s})[a_{31}(\sqrt{s})]$, which come after unitarization, are shown. The thin lines correspond to the following potentials which we finally use:

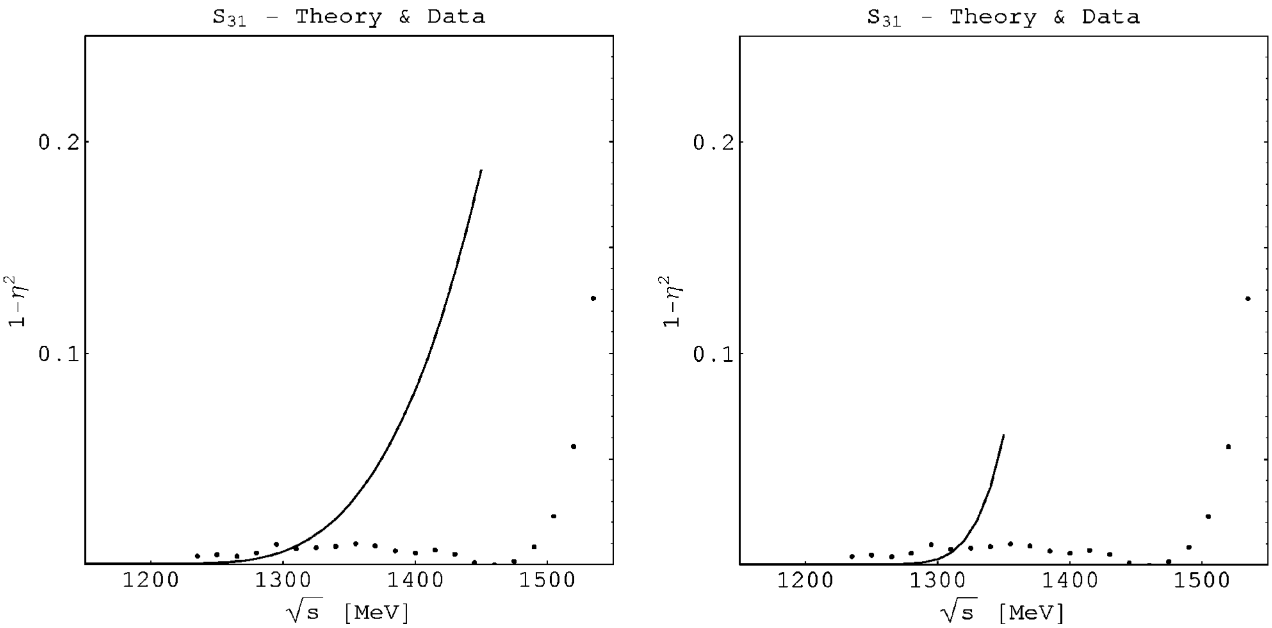

FIG. 15. Inelasticities of S_{31} πN scattering which correspond to the empirical $\pi N \rightarrow \pi\pi N$ amplitudes. The solids line in the left and right correspond to Ref. [23] and [24], respectively. The dotted line is the experimental analysis (Ref. [26]).

$$v_{11}(\sqrt{s}) = 4.0 + 1.0(\sqrt{s} - 1213)/m_\pi \ [m_\pi^{-3}], \qquad (29)$$

$$\begin{aligned} v_{31}(\sqrt{s}) = & -5.60(\sqrt{s}-1470)/m_\pi - 1.05(\sqrt{s}-1470)^2/m_\pi^2 \\ & + 1.77(\sqrt{s}-1470)^3/m_\pi^3 + 0.66(\sqrt{s}-1470)^4/m_\pi^4 \\ & - 0.17(\sqrt{s}-1470)^5/m_\pi^5 \\ & - 0.07(\sqrt{s}-1470)^6/m_\pi^6 \ [m_\pi^{-3}]. \qquad (30) \end{aligned}$$

The continuous line and dashed line correspond to the real and imaginary parts of $a_{11}(\sqrt{s})[a_{31}(\sqrt{s})]$, respectively. One can see that the imaginary parts are almost negligible as assumed in Refs. [23] and [24]. In the lower two graphs, the real part of $a_{11}(\sqrt{s})[a_{31}(\sqrt{s})]$ is plotted in comparison with the two empirical ones. The lower energy part of the calculated $a_{11}(\sqrt{s})$ agrees with that of Ref. [24] but it is quite different from the one of Ref. [23]. On the other hand our calculated $a_{31}(\sqrt{s})$ amplitude is different from both Ref. [23] and [24]. We should note that, while it is possible to reproduce the $\pi N \rightarrow \pi\pi N$ cross sections with the three set of amplitudes, a simultaneous description of the $\pi N \rightarrow \pi\pi N$ cross sections and the $\pi N \rightarrow \pi N$ scattering data is not possible with the amplitude of Ref. [23] and [24]. We shall elaborate further on this issue below.

The T-matrix elements obtained are shown in Fig. 13. One can see that the T-matrix elements are fairly reproduced at energies below 1600 MeV in both the S_{11} and S_{31} cases. The phase shifts and inelasticities are shown in Fig. 14. The inclusion of the $\pi\pi N$ channels improves slightly the phase shifts in S_{11} and S_{31}. The important thing to note is that, as seen in Fig. 14, the inelasticities at low energies in both S_{11} and S_{31} are well reproduced with the inclusion of the $\pi\pi N$ channels. The present $a_{11}(\sqrt{s})$ function is essentially the same as that of Ref. [24] in the range of energies studied there. Should we take the amplitude of Ref. [23], the inelasticities would be much overestimated at energies around 1400 MeV. The present $a_{31}(\sqrt{s})$ amplitude is different from both empirical $a_{31}(\sqrt{s})$ determinations. It has a node at the energy 1470 MeV which is reflected in the inelasticities shown in the figure. The inelasticities are quite sensitive to the $a_{31}(\sqrt{s})$ amplitude used. For example, the two empirical $a_{31}(\sqrt{s})$ correspond to the inelasticities shown in Fig. 15 which differ appreciably from those obtained with the function determined here. We should note that for this test we have used a function $v_{31}(\sqrt{s})$ such that after unitarization it leads to scattering amplitudes identical to the empirical $a_{31}(\sqrt{s})$. The unitarization procedure modifies only slightly the potential as is visible in upper right box of Fig. 12 for our case. The opposite sign of our $a_{31}(\sqrt{s})$ also provides the same inelasticities and hence is compatible with the S_{31} πN scattering data. However, it leads to unacceptable results for the $\pi N \rightarrow \pi\pi N$ cross section.

Figure 16 shows the $\pi N \rightarrow \pi\pi N$ cross sections. They are calculated with the present S-wave amplitudes and the P-wave amplitudes of Ref. [23]. The dashed lines correspond to the cross section when we drop the S-wave contributions. The two processes, $\pi^- p \rightarrow \pi^0\pi^0 n$ and $\pi^+ p \rightarrow \pi^+\pi^+ n$, are purely P wave πN and have no S-wave πN contribution. In the $\pi^- p \rightarrow \pi^+\pi^- n$ reaction, the P-wave contribution is large and dominates the process. The effect of the S wave is not visible in the figure. However, in the $\pi^- p \rightarrow \pi^0\pi^- p$ and $\pi^+ p \rightarrow \pi^0\pi^+ p$ processes we can see that the P-wave contributions are small and do not explain the size of the data. As one can see, the present S-wave amplitude provides enough strength to account for the cross section data. In the $\pi^- p \rightarrow \pi^0\pi^- p$ process, the S-wave amplitude is a mixture of $a_{11}(\sqrt{s})$ and $a_{31}(\sqrt{s})$. In order to obtain the contribution of the S wave shown in the figure, the amplitudes $a_{11}(\sqrt{s})$

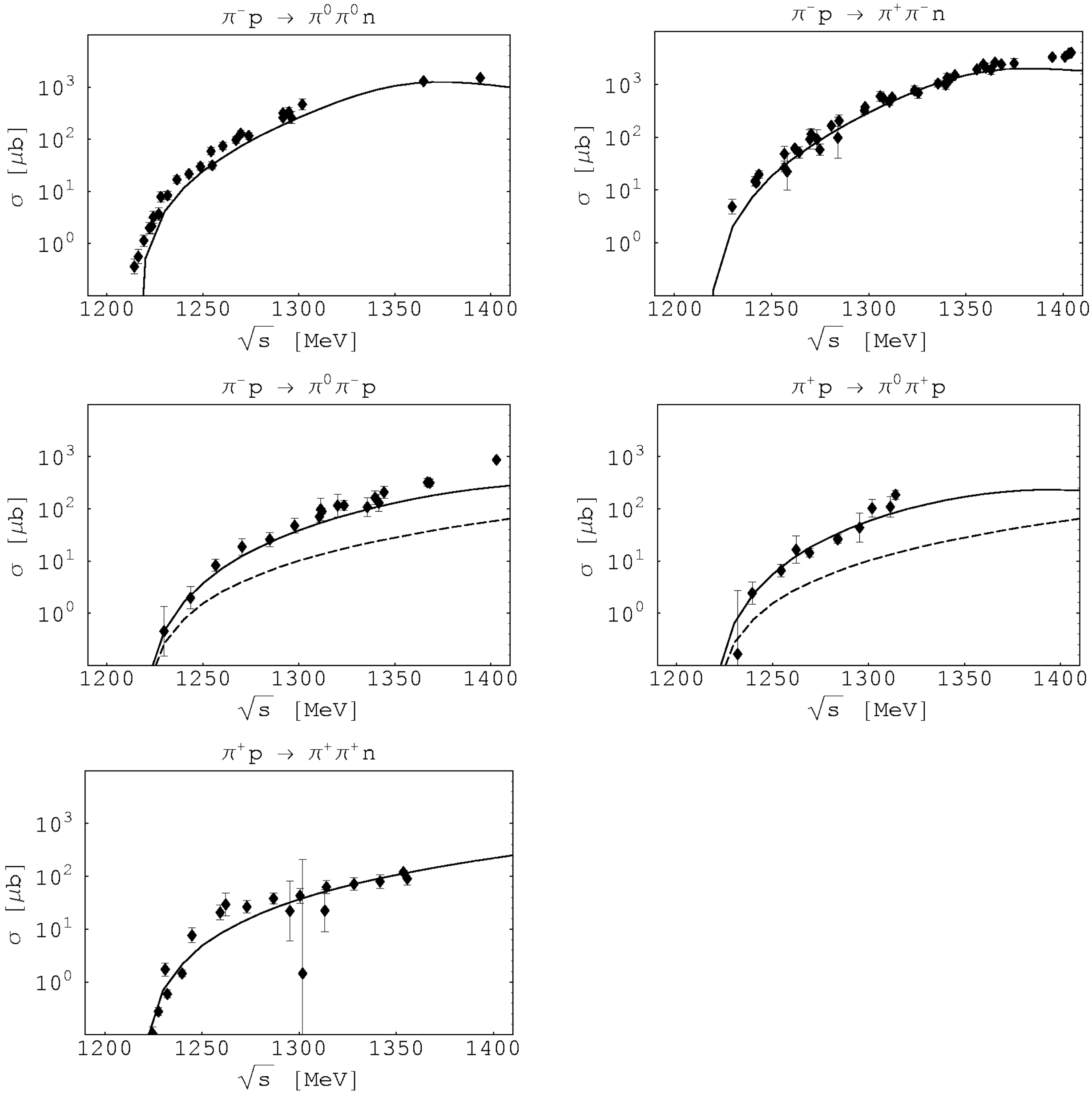

FIG. 16. The cross sections of $\pi N \to \pi\pi N$ scattering. Data points are taken from Ref. [24].

and $a_{31}(\sqrt{s})$ should interfere constructively close to the $\pi\pi N$ threshold. The relative sign between $a_{11}(\sqrt{s})$ and $a_{31}(\sqrt{s})$ [$v_{11}(\sqrt{s})$ and $v_{31}(\sqrt{s})$] is determined by this condition. The value of a_{11}/a_{31} at threshold is about $+1/2$, which is in contrast to the one pion exchange prediction, -2 [32]. However, more elaborate models for two pion production [33–38] contain many more terms that change the value of this ratio. The amplitudes $a_{11}(\sqrt{s})$ and $a_{31}(\sqrt{s})$ determined in this study account for both the πN elastic scattering data and the $\pi N \to \pi\pi N$ cross section data simultaneously.

In Fig. 17 we also show the result for the $\pi^- p \to \eta n$ cross section. We can see that the agreement is good up to 1550 MeV, above which higher partial waves, as demonstrated in Ref. [39], become relevant. We have also evaluated the scattering lengths in our approach which are listed in Table II. The thresholds for the $K^0\Lambda$, $K^0\Sigma^0$, and $K^+\Sigma^-$ are $\sqrt{s}$ $=1613$, 1690, and 1691 MeV, respectively. These energies, particularly the last two, are already in the region of energies where the theory deviates from experiment in the phase shifts and inelasticities, therefore we should take these numbers only as indicative. On the other hand, the fitting to the data has been done around the $N^*(1535)$ energy. Thus, our prediction for the ηn scattering length, $a_{\eta n} = 0.26 + i0.25$ fm, should be rather accurate. This number is in agreement with the result quoted in Ref. [8], $a_{\eta n} = 0.20 + i0.26$ fm, although a bit more attractive. Still, the real part is about a factor of 3 smaller than in Ref. [22] and a factor of 4 smaller than in Ref. [40]. In spite of that, it was argued in Ref. [8] that even the small value $\mathrm{Re}[a_{\eta n}] = 0.2$ fm is not unrealistically small. This scattering length is important since it plays a crucial role in the possibility to have η bound states in nuclei [41,42]. The scattering lengths for $\pi^0 n$ and

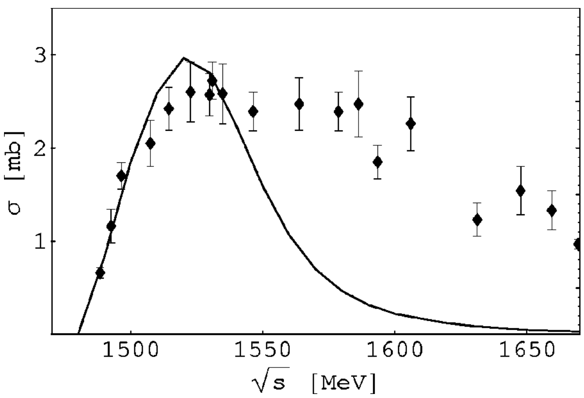

FIG. 17. The cross section of $\pi N \to \eta n$ scattering.

$\pi^- p$ have not been imposed in the fit to the data, which was concentrated in the $N^*(1535)$ region, as already mentioned. In this sense, the agreement with the data about 450 MeV below that resonance should be considered an unexpected success. We obtain isospin 3/2 and isospin 1/2 scattering lengths $a_3 = -0.0875\, m_\pi^{-1}$, $a_1 = 0.1272\, m_\pi^{-1}$, to be compared with the experimental numbers [43] $a_3^{exp} = -0.0852 \pm 0.0027\, m_\pi^{-1}$, $a_1^{exp} = 0.1752 \pm 0.0041\, m_\pi^{-1}$. The agreement is good for the isospin 3/2 scattering length, but the isospin 1/2 one is about 25% smaller than experiment.

To summarize the result of Secs. II and III, we can see that the chiral unitary approach including the $\pi\pi N$ channels is a very efficient tool to study the *S*-wave πN scattering. It can reproduce, with few parameters, not only the isospin 1/2 part but also the isospin 3/2 part, which could not be obtained before [6,20,21], when only meson-baryon channels were considered. Particularly, the $\pi\pi N$ channel was found essential to reproduce the isospin 3/2 scattering.

IV. THE $N^*(1535)$ AND $\Delta(1620)$ RESONANCES

As shown in Fig. 13, the calculated $T(S_{11})$ has a resonance behavior around 1535 MeV indicating that the well known negative parity baryon $N^*(1535)$ is generated in this approach. To find the pole corresponding to the resonance we extend our calculation of the T matrix to the complex P_0 plane. We evaluate the T-matrix elements by means of

$$T(P_0) = [V(P_0)^{-1} - G(P_0)]^{-1} \tag{31}$$

and look for poles in the complex P_0 plane. In this plane the function $G(P_0)$ has cuts on the real axis. For example, the left of Fig. 18 shows $\mathrm{Im}[G_{\pi^- p}(P_0)]$ in the physical sheet, namely, the first Riemann sheet. We also plot to the right of Fig. 18 the sheet connecting the first Riemann sheet for $\mathrm{Im}[P_0] \geq 0$ with the second Riemann sheet for $\mathrm{Im}[P_0] < 0$, which is defined as

$$G_i^{II}(P_0) = \begin{cases} G_i^I(P_0) & \text{at} \quad \mathrm{Re}[P_0] \leq \sqrt{s^0}_i\,, \\ G_i^I(P_0) - 2i\,\mathrm{Im}[G_i^I(P_0)] & \text{at} \quad \mathrm{Re}[P_0] > \sqrt{s^0}_i \end{cases} \tag{32}$$

with $\sqrt{s^0}_i$ the ith channel threshold energy. We need also to extrapolate $\tilde{G}(\sqrt{s})$ to the complex plane. For this purpose we parametrize the result for $\mathrm{Im}[\tilde{G}(\sqrt{s})]$ above the $\pi\pi N$ threshold in the real axis as

$$\begin{aligned} \mathrm{Im}[\tilde{G}(\sqrt{s})] = &-0.638(\sqrt{s} - 1213)/m_\pi \\ &+ 1.124(\sqrt{s} - 1213)^2/m_\pi^2 \\ &- 0.882(\sqrt{s} - 1213)^3/m_\pi^3, \end{aligned} \tag{33}$$

which allows for an analytical continuation for $\mathrm{Re}[P_0]$ above that threshold.

We search for poles of the isospin 1/2 T-matrix elements on this sheet, and obtain a pole at

$$P_0^R \equiv 1543 - i46 \;\; \text{MeV}. \tag{34}$$

The structure of the T matrix guarantees that we find the pole in all the elements which have an isospin 1/2 component. For example, the left of Fig. 19 shows $|T(S_{11})|$, where we can see a pole clearly. This result tells us that the decay width of the resonance is about 93 MeV. This value is smaller than the Paricle Data Group (PDG) estimation of 100–250 MeV [44], but agrees with the new data from Beijing Electron-Positron Collider (BEPC), 95 ± 15 MeV [45].

On the other hand, in the elements of pure isospin 3/2 we find a pole around $1625 - i215$ MeV, which is reminiscent of the $\Delta(1620)$ resonance, although with a larger width than the nominal one of the PDG of about 120–160 MeV. In the right of Fig. 19 we show $|T(S_{31})|$, where a pole is clearly visible. We should consider the position of the pole only as qualitative in our approach since around $\sqrt{s} = 1600$ MeV is where we start having noticeable discrepancies with the data and furthermore we had to go far in the complex plane where the analytic extrapolation of the $\pi\pi N$ loop function becomes less accurate. This resonance is responsible for the change of curvature in $\mathrm{Im}T(S_{31})$ shown in Fig. 13. It is interesting to note that the introduction of the $\pi\pi N$ channels is what has induced the appearance of this resonance, which does not show in our approach when the $\pi\pi N$ channels are not considered. In this respect it is interesting to note that the $\Delta(1620)$ resonance couples mostly to the $\pi\pi N$ channel [44].

For P_0 near the pole the T-matrix elements are approximated by

$$T_{ij}(P_0) \simeq \frac{g_i g_j}{P_0 - P_0^R} \tag{35}$$

TABLE II. The calculated meson-baryon scattering lengths in units of femtometers.

	$\pi^0 n$	$\pi^- p$	ηn	$K^0\Lambda$	$K^0\Sigma^0$	$K^+\Sigma^-$
a_i (fm)	-0.023	$0.080 + i0.003$	$0.264 + i0.245$	$-0.148 + i0.165$	$-0.205 + i0.068$	$-0.284 + i0.090$

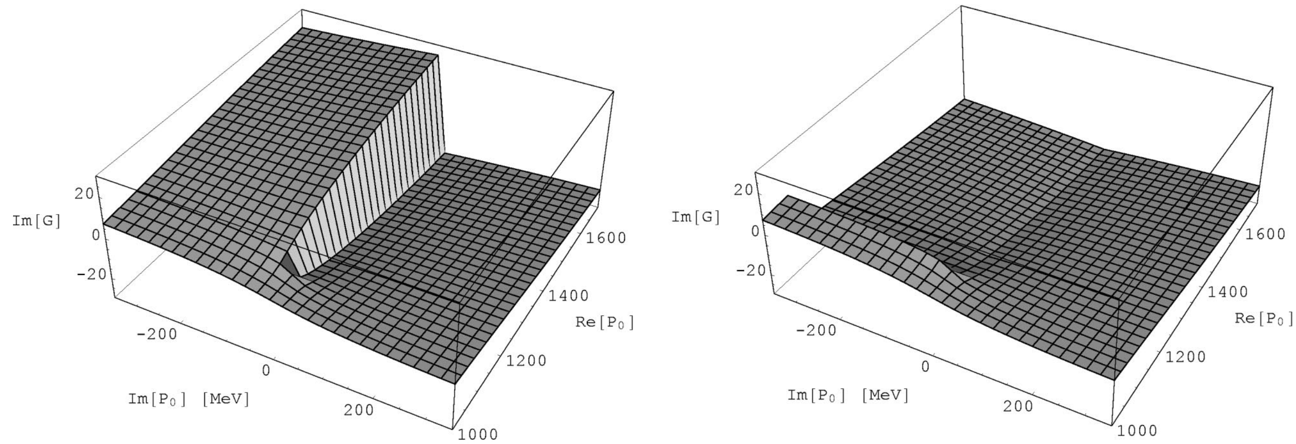

FIG. 18. The imaginary part of the loop function for the $\pi^- p$ system.

with g_i the couplings of the resonance to the ith channel. We obtain the size of the couplings by evaluating the residues of the diagonal elements $T_{ii}(P_0)$. The values obtained are listed in Table III. We find that the resonance $N^*(1535)$ couples strongly to the $K\Sigma$ and ηn channels with couplings four times larger than those for the πN channels. The couplings to the $K\Lambda$ are also large compared to the πN channels. In short, we get

$$|g_{\pi N}| < |g_{K\Lambda}| < |g_{\eta n}| \sim |g_{K\Sigma}|. \tag{36}$$

Using these couplings we calculate the partial decay widths of the open channels by means of

$$\Gamma_i = -2\,\mathrm{Im}[G_i(M_{N^*})]|g_i|^2, \tag{37}$$

where we take $M_{N^*} = \mathrm{Re}[P_0^R] = 1543$ MeV. The partial decay rates and the branching ratios obtained are also listed in Table III. The calculated branching ratios of πN, ηN, and $\pi\pi N$ decay modes are 22%, 70%, and 7%, respectively. The fraction of the ηN mode is large, which is known to be characteristic of this resonance although our fraction is bigger than the PDG estimation of 30–55%. Our πN fraction is smaller than the PDG estimation, 35–55%, while the $\pi\pi N$ fraction is compatible with the PDG estimation, $\leqslant 10\%$.

The lower part of Table III shows the same quantities obtained from a Breit-Wigner fit of the real energy scattering amplitudes $T_{ij}(\sqrt{s})$. We fit them by the Breit-Wigner form together with a background

$$T_{ij}(\sqrt{s}) = g_i g_j \frac{1}{\sqrt{s} - 1543 + i46} + a_{ij} + b_{ij}(\sqrt{s} - 1450) \tag{38}$$

at $1450 \leqslant \sqrt{s} \leqslant 1650$ MeV. The unknown parameters $g_i \times g_j$, a_{ij}, and b_{ij} are determined by the method of least squares. We obtain the values of g_i from the $g_{\eta n} \times g_i$ corresponding to the ηn final state amplitudes. Their absolute values agree fairly well with the values obtained from the pole residues and gives us confidence about our numerical evaluation of the couplings. For instance, the πN, ηn, and $\pi\pi N$ branching ratios are now 24%, 67%, and 9%, respectively.

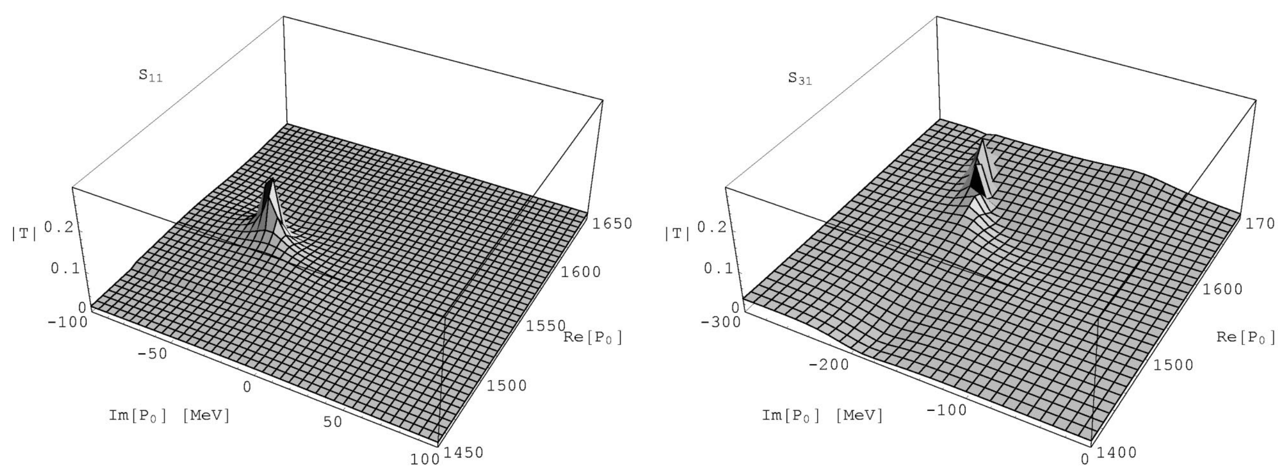

FIG. 19. $|T(S_{11})|$ (left) and $|T(S_{31})|$ (right) in the complex energy plane. The poles of $N^*(1535)$ and $\Delta(1620)$ are seen at the energies $1543 - i46$ MeV and $1625 - i215$ MeV, respectively.

TABLE III. Coupling constants and decay widths of $N^*(1535)$.

	$K^+\Sigma^-$	$K^0\Sigma^0$	$K^0\Lambda$	π^-p	π^0n	ηn	$\pi^0\pi^-p$	$\pi^+\pi^-n$
$\lvert g_i\rvert$	2.12	1.50	0.92	0.56	0.39	1.84	0.57 m_π^{-2}	0.40 m_π^{-2}
Γ_i (MeV)				14.1	7.0	65.7	4.6	2.4
Branching ratio (%)				15.0	7.4	70.1	4.9	2.5
g_i	−2.36	1.67	−1.28	−0.57	0.39	1.77	−0.61 m_π^{-2}	−0.43 m_π^{-2}
Γ_i (MeV)				15.0	7.1	60.8	5.4	2.6
Branching ratio (%)				16.5	7.8	66.9	5.9	2.9

This latter analysis allows us to determine the sign of the couplings. The signs given are relative to that of $g_{\eta n}$. It is instructive to decompose the resonance in the SU(3) representations. In fact, our result, ignoring the coupling to the $\pi\pi N$ channel, leads to

$$g_8=-2.52,\ \ g_{8'}=2.62,\ \ g_{10}=0.43,\ \ g_{27}=-0.47 \quad (39)$$

and tells us that the $N^*(1535)$ resonance is almost an equal weight mixture of the R-parity even SU(3) octet 8 and the R-parity odd SU(3) octet $8'$. It would be interesting to compare these results with the results from other models or lattice QCD simulations.

V. CONCLUSIONS

We have studied the S-wave πN scattering, together with that of coupled channels, in a chiral unitary model in the region of center of mass energies from threshold to 1600 MeV. We calculated the T matrix using the Bethe-Salpeter equation in the eight coupled channels including six meson-baryon channels and two $\pi\pi N$ channels. We took the transition potentials between the meson-baryon systems from the lowest order chiral Lagrangian and improved them taking into account the vector meson dominance hypothesis. Then we introduced the appropriate $\pi N \leftrightarrow \pi\pi N$ transition potentials which influence both the elastic scattering and the pion production processes. In the present model the renormalization due to higher order contributions is included by means of subtraction constants in the real part of the loop functions of the two- or three-body systems, which are taken as free parameters and determined through comparison with the T matrix of the data analysis. The imaginary part of the meson-baryon or $\pi\pi N$ loop functions is fixed and ensures unitarity in the S matrix. A realistic T matrix is obtained with a few free parameters for energies up to 1600 MeV. The phase shifts and the inelasticities up to 1600 MeV are fairly reproduced, particularly taking into account the limited amount of free parameters. The agreement is somewhat worse in the isospin 3/2 channel but in any case this represents a considerable improvement with respect to earlier works where the $\pi\pi N$ channels were omitted. We find that the correction of the chiral coefficient and the $\pi\pi N$ channels are important to obtain a more accurate T matrix, especially in isospin 3/2. Our analysis allowed us to determine the S-wave amplitudes for $\pi N \rightarrow \pi\pi N$ and we found that the isospin 3/2 $\pi N \leftrightarrow \pi\pi N$ amplitude is different from the two previous empirical ones.

The resonance $N^*(1535)$ is generated dynamically and qualifies as a quasibound state of meson and baryon. The corresponding pole is seen in the T matrix on the complex plane. We calculate the total and partial decay widths of the resonance. The total width obtained, about 80 MeV, is smaller than the PDG estimation, but agrees with the new data from BEPC. Also the large ηn branching ratio observed in the data is reproduced.

The present study has served to show the potential of the chiral unitary approach extending the predictions to higher energies than would be possible with the use of χPT. Yet, we also saw that improvements in the basic information of the lowest order chiral Lagrangians to account for phenomenology of VMD are welcome. On the other hand we found mandatory the inclusion of the $\pi\pi N$ channels in order to find a more accurate reproduction of the data, particularly those in the isospin 3/2 sector. We also found that the introduction of these channels, forcing them to reproduce the inelasticities and other data, has as an indirect consequence that the $\Delta(1620)$ resonance appears then as a pole in the complex plane indicating a large mixing of this resonance with $\pi\pi N$ states. This interpretation would be consistent with the large experimental coupling of this resonance to the $\pi\pi N$ channel.

ACKNOWLEDGMENTS

We would like to acknowledge discussions with J. C. Nácher. One of us, T.I., would like to thank J. A. Oller and A. Hosaka for useful discussions. This work was partly supported by the Spanish Ministry of Education in the program ''Estancias de Doctores y Tecnólogos Extranjeros en España,'' by DGICYT Contract No. BFM2000-1326, and by the EU TMR network Eurodaphne, Contract No. ERBFMRX-CT98-0169.

[1] J. Gasser and H. Leutwyler, Nucl. Phys. **B250**, 465 (1985).
[2] U.G. Meissner, Rep. Prog. Phys. **56**, 903 (1993).
[3] V. Bernard, N. Kaiser, and U.G. Meissner, Int. J. Mod. Phys. E **4**, 193 (1995).
[4] A. Pich, Rep. Prog. Phys. **58**, 563 (1995).
[5] G. Ecker, Prog. Part. Nucl. Phys. **35**, 1 (1995).
[6] N. Kaiser, P.B. Siegel, and W. Weise, Phys. Lett. B **362**, 23 (1995).
[7] N. Kaiser, P.B. Siegel, and W. Weise, Nucl. Phys. **A594**, 325 (1995).
[8] N. Kaiser, T. Waas, and W. Weise, Nucl. Phys. **A612**, 297 (1997).
[9] J.A. Oller and E. Oset, Nucl. Phys. **A620**, 438 (1997); **A652**, 407(E) (1999).
[10] J.A. Oller, E. Oset, and J.R. Peláez, Phys. Rev. D **59**, 074001 (1999); **60**, 099906(E) (1999).
[11] J.A. Oller and E. Oset, Phys. Rev. D **60**, 074023 (1999).
[12] A. Gómez Nicola and J.R. Peláez, Phys. Rev. D **62**, 017502 (2000).
[13] A. Gómez Nicola, J. Nieves, J.R. Peláez, and E. Ruiz Arriola, Phys. Lett. B **486**, 77 (2000).
[14] U.G. Meissner and J.A. Oller, Nucl. Phys. **A673**, 311 (2000).
[15] J.A Oller and U.G. Meissner, Phys. Lett. B **500**, 263 (2001).
[16] J.A. Oller, E. Oset, and A. Ramos, Prog. Part. Nucl. Phys. **45**, 157 (2000).
[17] T.P. Vrana, S.A. Dytman, and T.S.H. Lee, Phys. Rep. **328**, 181 (2000).
[18] T. Feuster and U. Mosel, Phys. Rev. C **58**, 457 (1998).
[19] E. Oset and A. Ramos, Nucl. Phys. **A635**, 99 (1998).
[20] J.C. Nácher, A. Parreño, E. Oset, A. Ramos, A. Hosaka, and M. Oka, Nucl. Phys. **A678**, 187 (2000).
[21] J. Nieves and E. Ruiz Arriola, Phys. Rev. D **64**, 116008 (2001).
[22] A.M. Green and S. Wycech, Phys. Rev. C **60**, 035208 (1999).
[23] D.M. Manley, Phys. Rev. D **30**, 536 (1984).
[24] H. Burkhardt and J. Lowe, Phys. Rev. Lett. **67**, 2622 (1991).
[25] F. Mandl and G. Show, *Quantum Field Theory* (Wiley, New York, 1984).
[26] Center of Nuclear Study, World Wide Web site http://gwdac.phys.gwu.edu/
[27] G. Ecker, J. Gasser, A. Pich, and E. de Rafael, Nucl. Phys. **B321**, 311 (1989).
[28] J. Nieves and E. Ruiz Arriola, Phys. Lett. B **455**, 30 (1999).
[29] J. Nieves and E. Ruiz Arriola, Nucl. Phys. **A679**, 57 (2000).
[30] M. Urban, M. Buballa, and J. Wambach, Nucl. Phys. **A641**, 433 (1998).
[31] F. Klingl, N. Kaiser, and W. Weise, Z. Phys. A **356**, 193 (1996).
[32] R. Aaron, *et al.*, Phys. Rev. D **16**, 50 (1977).
[33] E. Oset and M.J. Vicente Vacas, Nucl. Phys. **A446**, 584 (1985).
[34] V. Sossi, N. Fazel, R.R. Johnson, and M.J. Vicente Vacas, Phys. Lett. B **298**, 287 (1993).
[35] O. Jaekel, M. Dillig, and C.A.Z. Vasconcellos, Nucl. Phys. **A541**, 675 (1992).
[36] V. Bernard, N. Kaiser, and U.G. Meissner, Nucl. Phys. **B457**, 147 (1995).
[37] V. Bernard, N. Kaiser, and U.G. Meissner, Nucl. Phys. **A619**, 261 (1997).
[38] T.S. Jensen and A.F. Miranda, Phys. Rev. C **55**, 1039 (1997).
[39] J. Caro Ramon, N. Kaiser, S. Wetzes, and W. Weise, Nucl. Phys. **A672**, 249 (2000).
[40] M. Batinic, I. Slaus, and A. Svarc, Phys. Rev. C **52**, 2188 (1995).
[41] H.C. Chiang, E. Oset, and L.C. Liu, Phys. Rev. C **44**, 738 (1991).
[42] R.S. Hayano, S. Hirenzaki, and A. Gillitzer, Eur. Phys. J. A **6**, 99 (1999).
[43] H.-Ch. Schröder *et al.*, Phys. Lett. B **469**, 25 (1999).
[44] Particle Data Group, D.E. Groom *et al.*, Eur. Phys. J. C **15**, 1 (2000).
[45] J.Z. Bai *et al.*, Phys. Lett. B **510**, 75 (2001).